THE JOURNAL OF PHYSICAL CHEMISTRY C

Article

Cite This: J. Phys. Chem. C 2018, 122, 21686−21693

pubs.acs.org/JPCC

Subnanometer Substructures in Nanoassemblies Formed from Clusters under a Reactive Atmosphere Revealed Using Machine Learning

Janis Timoshenko,*[,†] Avik Halder,[‡] Bing Yang,[‡] Soenke Seifert,[§] Michael J. Pellin,[‡] Stefan Vajda,[‡,∥] and Anatoly I. Frenkel*[,†,⊥]

[†]Department of Materials Science and Chemical Engineering, Stony Brook University, Stony Brook, New York 11794, United States

[‡]Materials Science Division and [§]X-ray Science Division, Argonne National Laboratory, 9700 South Cass Avenue, Argonne, Illinois 60439, United States

[∥]Institute for Molecular Engineering, The University of Chicago, 5640 South Ellis Avenue, Chicago, Illinois 60637, United States

[⊥]Chemistry Department, Brookhaven National Laboratory, Upton, New York 11973, United States

Supporting Information

ABSTRACT: Size-selected clusters, soft-landed on an oxide substrate, is a promising and highly tunable material for heterogeneous catalysis. Agglomeration of the deposited clusters, however, leads to changes in the particle properties and structure. The latter for such cluster assemblies can also be different from that in self-standing nanoparticles of similar sizes. To monitor the formation of such complex materials, in situ studies at different length scales are required. Toward that goal, we combined small-angle X-ray scattering (SAXS), X-ray absorption near-edge structure (XANES) spectroscopy, ab initio simulations, and machine learning (artificial neural network) techniques. We detected significant differences between the sizes of particle agglomerates, as probed by SAXS, and the sizes of locally ordered regions, as seen by XANES. We interpret these differences as an evidence for the fractal, grape-cluster-like structure of the agglomerates; thus, XANES and SAXS provide highly complementary structural information. This finding can have a profound effect on our understanding of particle sintering and assembly processes and of structure−properties relationship in ultradispersed metal catalysts in reaction conditions.

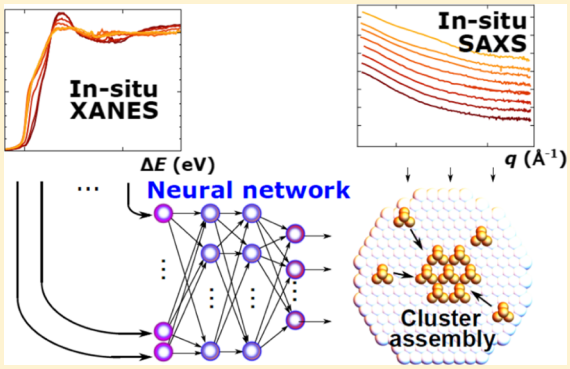

1. INTRODUCTION

Structures and shapes of subnanometer size-selected clusters are predicted to vary within a wide range of possible motifs, in a striking contrast with much fewer possibilities for nanoparticles (NPs) in the 1 nm and larger size range.[1−8] The resulting properties of the clusters are unique and can change dramatically and nonmonotonically upon changes in cluster size, often by an addition or removal of a single atom.[9−12] In particular, unique catalytic properties have been recently observed for such materials.[4,6,9,10,13−19] To benefit from these properties for application to heterogenous catalysis, the size-selected clusters produced in the gas phase can be soft-landed on suitable support materials.[6,9] The interactions between support and deposited clusters can have a significant effect on the properties of the clusters and can be used to further tailor the properties of the catalyst.[9,17,20−22]

Other complications that may arise, when well-defined clusters are extracted from the gas phase, are the cluster−cluster interactions and agglomeration.[6,9] The deposited clusters may undergo coarsening (via the Ostwald ripening or diffusion−coalescence processes) that often occurs at elevated temperatures of catalytic reactions.[23] Importantly, depending on the ambient conditions, the latter coarsening mechanism may result in less compact, fractal structures. The properties of such cluster aggregates can be quite different from the properties of the close-packed NPs of similar size. Although typically agglomeration decreases the catalytic activity of nanocatalysts (because of the reduction of the number of active sites), controlled self-assembly of deposited clusters can be desirable for certain applications.[24,25] For example, higher catalytic selectivity was recently observed for aggregates of subnanometer silver clusters than for self-standing particles of similar size.[9,26,27]

To understand the structure−property relationship in such noncompact cluster aggregates, experimental tools are needed that allow one to probe the aggregate structure at different

Received: August 15, 2018
Revised: August 22, 2018
Published: August 26, 2018

DOI: 10.1021/acs.jpcc.8b07952
J. Phys. Chem. C 2018, 122, 21686−21693

length scales, corresponding to intracluster and intercluster dimensions. Because of the metastable nature of such systems and their high sensitivity to ambient conditions, it is important to monitor their formation in situ, under reaction conditions. Low metal loadings, high reaction temperatures, and the presence of a support hinder applications of many techniques, such as extended X-ray absorption fine structure (EXAFS) spectroscopy,[28,29] which is commonly used for studies of larger NPs.[30−33] Among the very few tools that could be used for studies of ultradispersed, size-selected clusters, a combination of grazing incidence small-angle X-ray scattering (GISAXS)[34] and grazing-incidence X-ray absorption near-edge structure (GIXANES) has proven to be especially powerful to quantify the size and ordering of catalytic clusters deposited on supports.[35] In this combined approach, GIXANES has been mostly employed to monitor the oxidation state of the clusters during the reaction,[9,18,35] whereas GISAXS is used as a tool to monitor the stability of clusters and to measure the average size (width and height) of the agglomerates when sintering takes place.[13,18,27,34−37] It is far from trivial, however, to extract from XANES and SAXS information about the inner structure of the cluster aggregates. We have recently demonstrated that machine-learning-based analysis of XANES can be used to probe the three-dimensional geometry of the NPs.[25,38] By employing an artificial neural network (NN) trained on a large set of theoretical XANES spectra, we were able to obtain metal−metal coordination numbers (CNs) and thus decipher the local structure in supported Pt NPs,[38] as well as to monitor the in situ formation of Ag particles from their experimental XANES spectra.[25]

In this work, we modified our machine-learning method to adapt it to the unique case of clusters in which more structural descriptors, such as interatomic distances, and not just CNs, are expected to affect their XANES spectra. By combining this method with GISAXS, we analyzed the multiscale structure of agglomerates of ultradispersed size-selected copper clusters. Copper-based nanomaterials have proven to be efficient catalysts for the conversion of carbon dioxide to value-added fuels and chemicals,[6,9,14,15,39−43] where the catalytic properties depend critically on the NP size.[6,9,14,15,43] Monitoring the NP growth under reaction conditions is thus important for understanding the working mechanism and designing new catalysts for CO_2 conversion. By employing XANES and SAXS methods, we are able to elucidate the details of the copper cluster agglomeration and its dependency on ambient conditions and the support material and to do so at different length scales in the same in situ experiment. Although SAXS probes the overall geometry of the agglomerate, the local sensitivity of XANES makes it ideally suited to probe its inner structure.

An additional important outcome of this analysis method is due to its sensitivity not just to the cluster size but to interatomic distances as well. It is known that the distances between nearest neighbors in metal NPs decrease with particle sizes.[44−47] This could have an important additional effect on the electronic structure[48,49] and the catalytic properties of NPs.[50,51] Shortening of interatomic distances can also be used as an independent indication of very small particle sizes,[46] especially if these distances can be extracted from XANES rather than EXAFS data. For the latter, the interpretation of changes in interatomic distances is often complicated by the artifacts in the data analysis because of the asymmetry of the bond-length distribution.[52−57] These problems affect XANES data interpretation to a much lesser extent.

2. METHOD DESCRIPTION

This sensitivity of Cu K-edge XANES to NP size has been demonstrated before by theoretical simulations.[58,59] We illustrate this effect in Figure 1, where we compare theoretically

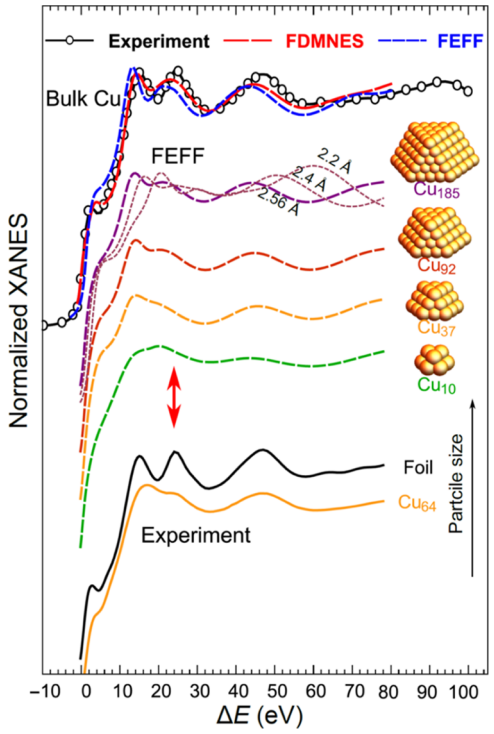

Figure 1. Experimental Cu K-edge XANES and theoretical spectra calculated with two ab initio XANES codes (FDMNES[62] and FEFF[60]) for bulk Cu and Cu clusters of different sizes. For the Cu_{185} cluster, the effect of interatomic distance is also demonstrated based on FEFF simulations. The red arrows mark the feature in XANES spectra that is very sensitive to particle size.

calculated (with FEFF code[60]) particle-averaged XANES spectra for Cu clusters of different sizes, as well as experimental reference spectra for bulk foil and Cu_{64} NPs, prepared via dendrimer-encapsulation method.[61] The details of XANES simulations are given in Supporting Information (Note 1). Both experimental and simulated data suggest that for smaller particles XANES spectra are relatively smooth and featureless. A similar effect was observed in our previous work on Pt clusters,[38] where it was attributed to the contribution of undercoordinated surface atoms. Upon increase of NP size, XANES features get more pronounced, and for a particle with a few hundreds of atoms, they can resemble those in bulk Cu. For very small clusters, a particularly sensitive characteristic of their size is the lack of the feature at ca 20 eV above the absorption edge (Figure 1). As shown in Figure 1 (and demonstrated in refs[20,58,59]), this feature is absent in clusters with ca. 20 atoms or less but is present in larger clusters. In addition to the particle size effect, Figure 1 also demonstrates a pronounced effect of Cu−Cu interatomic distances on simulated XANES spectra (also acknowledged before[58]). Finally, we note that, when the experimental data are compared with the results of simulations, they agree qualitatively, but some systematic deviations can be clearly

DOI: 10.1021/acs.jpcc.8b07952
J. Phys. Chem. C 2018, 122, 21686−21693

seen, as demonstrated in Figure 1, on the example of XANES spectra for bulk copper and simulations with two state-of-the-art codes, FEFF[60] and FDMNES.[62] These systematic deficiencies of XANES modeling are the known bottleneck of the method, hindering, in general, its application to quantitative studies of material structure. However, as we have demonstrated, this problem can be resolved by applying supervised machine-learning techniques, such as artificial NNs.[38]

We followed a procedure similar to that described in ref 38. Briefly, we used FEFF and FDMNES codes to generate site-specific XANES data for Cu particles of different sizes and shapes. As in our previous work,[38] for NN training, we do not use the particle-averaged spectra but an artificial data set created by randomly sampling and averaging site-specific theoretical XANES spectra for a small ensemble of 21 particles of different sizes and shapes (some are shown in Figure 2).

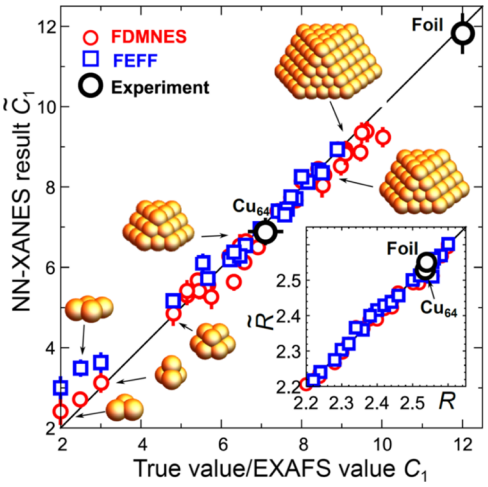

Figure 2. Validation of NN accuracy with theoretical particle-averaged XANES spectra and with experimental data. For theoretical data, obtained in FDMNES[62] and FEFF[60] simulations for Cu particles of different sizes, results of NN-XANES analysis (first-shell CN $\tilde{C}_1$ and nearest-neighbor distance $\tilde{R}$) are compared with the true values C_1 and R for the corresponding particle model. The units of the distance in the inset are Å. For experimental data, results of NN-XANES analysis are compared with the results of conventional EXAFS analysis.[61]

Theoretical XANES spectra $\mu(E)$ generated with FEFF and FDMNES codes are first aligned to match the energy scale used in theoretical calculations with the energy scale of experimental data by shifting the calculated spectra by ΔE. The values of ΔE (different for FEFF and FDMNES) are chosen so that the experimental and calculated Cu K-edge XANES for bulk Cu are aligned. Next, we reinterpolate the theoretical spectra on a nonuniform mesh that spans energies from E_{min} = 8986.9 eV to E_{max} = 9066.0 eV. The mesh step size is 0.2 eV for data points near the absorption edge and gradually increases up to 1.0 eV for points at $E = E_{max}$. The resulting $\vec{\mu}$ vector contains 115 data points μ_i corresponding to the values of the absorption coefficient at different energies E_i. Finally, as explained in our previous work,[38] we subtract from the vector that corresponds to the calculated spectrum for the copper cluster the vector $\vec{\mu}_{bulk}$ that corresponds to the calculated spectrum for bulk copper to minimize systematic errors due to background modeling. The difference vector $\Delta\vec{\mu} = \vec{\mu} - \vec{\mu}_{bulk}$ with 115 data points is then directly used to initialize the values of 115 nodes in the input layer of our NN. No additional dimensionality reduction, normalization, feature selection, or peak identification is carried out.

Regular Cu NPs structure models with a fcc-type structure and with octahedral, truncated octahedral, cuboctahedral, and cubic shapes that were used to generate XANES spectra for NN training were constructed by cutting with a (100) and (111) plane fcc-type Cu lattice with lattice constant a_0 = 3.615 Å.[63] These regular structures were further truncated with an additional (100) or (111) plane to model an interface with a substrate. To partially account for possible deviations from close-packed (here: fcc-type) atom arrangements, we also include in the training data set regular icosahedral- and hcp-type clusters constructed using a cluster coordinate generator,[64] maintaining the same nearest-neighbor distance 2.556 Å as in fcc-type clusters. Each cluster model in our set can be uniquely characterized by a set of average CNs for the first few coordination shells $\{C_1, C_2, C_3,...\}$.[64] In addition, because here for the first time we explore also the sensitivity of the NN-XANES method to interatomic distances, we constructed additional structure models by isotropically stretching or compressing the clusters with respect to the original set so that the distance between nearest neighbors R changed between 2.2 and 2.6 Å. The lower limit corresponds to the expected Cu−Cu distance in the Cu dimer,[65] whereas the upper limit for the Cu−Cu distance is chosen so that it exceeds slightly the bulk value. As a result, NN will be trained on a broad range of distances, encompassing the possible distances in actual clusters.

We construct a NN as a composite nonlinear function $h(\mu^i,\vec{\theta}) \rightarrow \{\tilde{C}_1, \tilde{C}_2, \tilde{C}_3,...,\tilde{R}\}^i$ that uses as input a preprocessed and discretized XANES spectrum μ^i, depends on parameters described by the vector $\vec{\theta}$ and returns a vector $\{\tilde{C}_1, \tilde{C}_2, \tilde{C}_3,...,\tilde{R}\}^i$. During the training process, we supply as input for NN the theoretical XANES spectra (for which the true structure parameters $\{C_1, C_2, C_3,...,R\}^i$ are known) and fit the NN parameters $\vec{\theta}$ so that the Euclidean distance between the true structure parameter vector and NN output vector $\{\tilde{C}_1, \tilde{C}_2, \tilde{C}_3,...,\tilde{R}\}^i$ is minimized for all spectra in our training set. After the optimal values of $\vec{\theta}$ are found, NN can take experimental XANES as an input and determine $\{\tilde{C}_1, \tilde{C}_2, \tilde{C}_3,...,\tilde{R}\}$ as estimators for average CNs and interatomic nearest-neighbor distance for NPs in the corresponding sample. Average CNs, in turn, can be immediately linked to the effective particle size.[30,32] More details on the construction of the training data set and NN design and training are given in Supporting Information (Note 2) and in refs.[25,38,66]

To validate the accuracy of the trained NN, we have relied on theoretical XANES data, calculated by FEFF and FDMNES codes for particles of different sizes and shapes (Figure 2). Unlike it was for the NN training step, for validation, we use particle-averaged XANES spectra, corresponding to realistic Cu particles. We include structure models, indirectly used for NN training, as well as the structure models that were not used for the construction of the training data set. To validate the ability of our NN to predict also the interatomic distances, we included in the validation data set structure models with different interatomic distances.

In Figure 2, the true values of CNs for the first coordination shell and the true values of Cu−Cu distance are compared with the ones yielded by NN from the corresponding XANES data. The validation results for more distant coordination shells

DOI: 10.1021/acs.jpcc.8b07952
J. Phys. Chem. C 2018, 122, 21686−21693

(also accessible, in principle, by our NN method) are given in the Supporting Information (Figure S1). As one can see, the structure parameters, determined by NN, agree well with the true values for a broad range of particle sizes and interatomic distances. Importantly, our NN is able to reproduce reliably also the low CN values for ultrasmall clusters with 3−4 atoms.

In addition, we have validated the accuracy of the NN-XANES method also with experimental Cu K-edge XANES data for well-defined samples, where the CN and R values are known from EXAFS analysis.[61] To apply our NN to experimental XANES data, we, first, align, merge, and normalize them using a standard procedure as implemented in ATHENA software.[67] Afterward, the spectra are processed in the same way as explained above for the theoretical spectra: the spectra are reinterpolated on the same energy mesh as used for theoretical spectra, and the experimental spectrum corresponding to bulk copper (copper foil) is subtracted. The resulting vector with 115 data points can be then directly processed by our NN. The results obtained by NN from experimental data for bulk copper and Cu_{64} NPs are also shown in Figure 2 and demonstrate the robustness of our NN toward systematic differences between experiment and theory.

After the accuracy of our NN is demonstrated using theoretical and experimental data, we can apply it to solve the unknown structure of supported ultrasmall size-selected copper clusters. We emphasize here that a good performance of our NN for this system was not guaranteed because the structure of such clusters can, in principle, deviate significantly from the close-packed model structures used for NN training and can also be affected by interactions with the support. Our method should be applied with caution in this case. Nevertheless, as we demonstrate below, in this particular case, our NN method provided reliable results.

3. RESULTS AND DISCUSSION

Cu_4, Cu_{12}, and Cu_{20} clusters were synthesized using a size-selected cluster source[14,15] and soft-landed on a thin layer of ZrO_2 or ZnO, prepared by the atomic layer deposition on the top of a silicon wafer.[68,69] To model the conditions of the CO_2 conversion reaction, the deposited clusters were exposed to the mixture of CO_2 and hydrogen in helium with the concentrations in the ratio 1:3:1 (with a few 100 ppm of O_2 and H_2O) and gradually heated up to 375 °C (see the inset in Figure 3). During the heating, in situ XANES and SAXS data were collected in GI mode. Experimental details are given in the Supporting Information (Note 3).

Temperature-dependent in situ XANES data for Cu_4 clusters on ZrO_2 are compared with the spectra of reference materials in Figure 3. Qualitatively similar temperature-dependencies of XANES spectra for Cu_4, Cu_{12}, and Cu_{20} clusters on ZrO_2, as well as for clusters on ZnO are shown in the Supporting Information (Figure S2). As one can see, in agreement with the previous studies,[14,15] the as-prepared clusters are oxidized, as evidenced by similar shapes and positions of the main features in XANES spectra to those for $Cu(OH)_2$. Upon heating, however, the samples are rapidly reduced. To quantify this process, we perform linear combination analysis by fitting all spectra for a particular sample with a linear combination of the spectrum for the as-prepared sample and the spectrum collected at the highest temperature (375 °C). The latter resembles qualitatively the spectrum of metallic copper, but all features are broadened, in agreement with the expected small particle size. The changes in the relative contribution of this

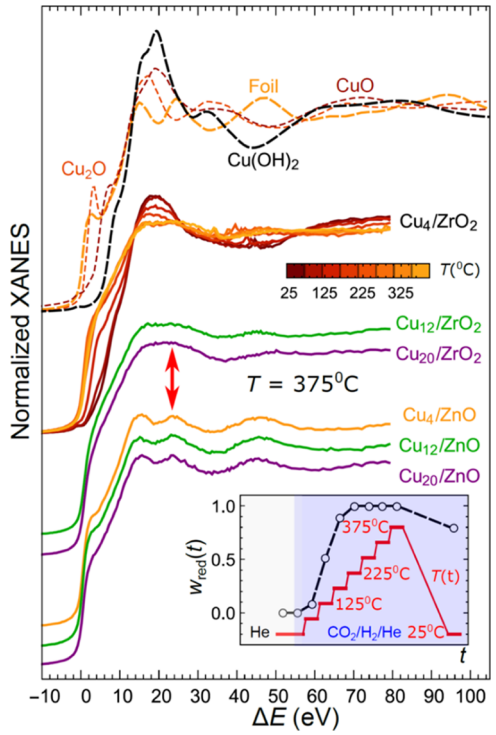

Figure 3. In situ XANES for size-selected clusters. Experimental, temperature-dependent XANES for Cu_4 clusters on ZrO_2 is compared with the spectra for reference materials and demonstrates an increase of reduced metal fraction w_{red} with temperature (see inset). High-temperature XANES data for Cu_4 on ZrO_2 are compared with those for Cu_{12} and Cu_{20} clusters, as well as for clusters on the ZnO support.

high-temperature spectrum (w_{red}) are reported in the inset of Figure 3. As one can see, after 225 °C, w_{red} reaches its maximal value and further heating does not affect it. We interpret this as an evidence that the sample is completely reduced at this temperature. Noteworthy, after the sample is cooled down to room temperature, it becomes partially reoxidized.

In Figure 3, we also compare the high-temperature (375 °C) spectrum for the Cu_4 cluster on zirconia with those for Cu_{12} and Cu_{20} clusters, as well as for clusters on ZnO. Strikingly, although the spectra for all clusters on zirconia are similar and have the same broad, featureless shapes, as expected for ultrasmall clusters (Figure 1), the spectra for clusters on ZnO, which nominally have the same size, are clearly different; features of metallic copper are much more pronounced here, as is also the size-sensitive feature at ca. 20 eV above the absorption edge (Figure 3). Thus, one can conclude immediately that the clusters on the ZnO support after reduction have significantly larger sizes than the clusters on zirconia support, which hints at the possibility of significant agglomeration of ZnO-supported clusters.

The CNs $\tilde{C}_1$, as well as interatomic distances $\tilde{R}$ extracted from XANES data for size-selected Cu clusters by NN method are shown in Figure 4. We focus here on the results obtained at high temperature because our NN method is, at present, applicable to reduced particles only. Note that the metallic state of copper is also relevant for many catalytic applications.[6,15]

The obtained NN-XANES results agree with the conclusions from the visual examination of experimental XANES data: CNs for all samples on ZnO are significantly larger than those for samples on ZrO_2. In fact, all three samples on ZnO have very

DOI: 10.1021/acs.jpcc.8b07952
J. Phys. Chem. C 2018, 122, 21686−21693

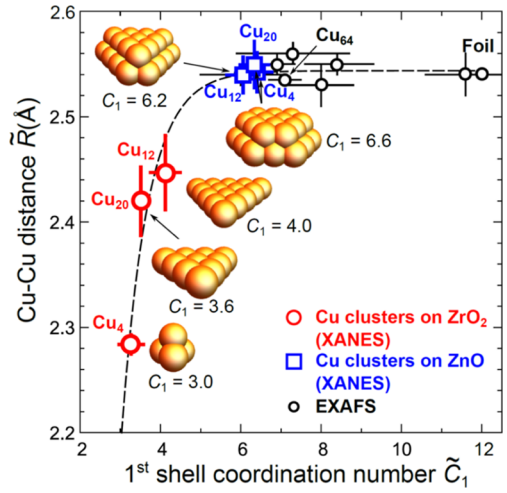

Figure 4. First-shell CNs and effective nearest-neighbor distances for size-selected clusters on ZrO_2 and ZnO, extracted by NN method from high-temperature (375 °C) XANES data. Next to symbols are also shown examples of possible particle models with the first-shell CNs, similar to those obtained from the analysis of experimental data. For completeness, the CNs and interatomic distances reported in the literature[20,61,65,70,71] for copper NPs of larger sizes (extracted from EXAFS analysis) are also shown. The dashed line is the guide to the eye.

similar CNs and also similar nearest-neighbor distances that are close to those for the Cu_{64} particle.

CNs for samples on zirconia are much closer to what is expected for clusters with nominally 4, 12, and 20 atoms, respectively. For the Cu_4 sample, the obtained CN (approximately, 3) is, in fact, in agreement with that for the close-packed arrangement of four atoms (Figure 4). Larger CNs (approximately, 4) are observed for Cu_{12} and Cu_{20} clusters. Among the possible structure models that have such CNs, one can mention planar clusters with 10−15 atoms, also shown in Figure 4.

In addition to CNs, also interatomic distances can be used for the determination of particle sizes because for small particles the shortening of interatomic distances is expected. Such an approach was applied, for example, in ref 46 for size determination of much larger Au particles. As shown in Figure 4, EXAFS data, available in the literature for NPs with CNs larger than 6,[20,61,65,70,71] indicate that the Cu−Cu distance does not change significantly with the particle size and is approximately the same as in bulk copper. As mentioned above, our NN-XANES results for clusters on the ZnO support agree well with these observations made on the basis of EXAFS data. For smaller clusters on zirconia, however, the Cu−Cu distance is significantly shorter and decreases systematically with the particle size (CN). In fact, the obtained Cu−Cu distance for Cu clusters on zirconia agrees well with the expected one for subnanometer clusters.[65] The fact that two independently obtained quantities—CNs and interatomic distances—extracted by our NN from experimental XANES data both point to the same conclusion regarding the ultrasmall size of Cu clusters on zirconia allows us to conclude that, first of all, the obtained results are reliable and, second, that the structure and charge state of clusters, investigated in this work, are not too different from those in close-packed models used for NN training (which is a noteworthy result by itself).

Information on particle sizes, obtained from XANES analysis, can be correlated with the results of GISAXS measurements. Experimental temperature-dependent GISAXS data (collected simultaneously with the XANES data) for Cu_4 clusters on ZrO_2 are shown in Figure 5a. GISAXS data for

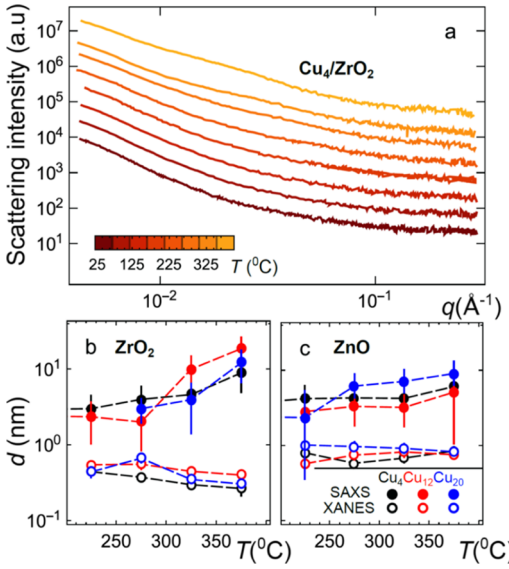

Figure 5. Temperature-dependent GISAXS data for Cu_4 clusters on ZrO_2 (a). Cluster diameters d estimated from GISAXS data for Cu_4 clusters on ZrO_2, as well as for Cu_{12} and Cu_{20} clusters, and clusters on the ZnO support are compared with NN-XANES results in (b) and (c). The dashed lines are guides to the eye. Note: the smallest resolvable particle size by GISAXS in this experiment is ~2 nm. At low temperatures, the sizes of the as-deposited clusters and their assemblies are below the GISAXS detection limit. As uncertainties for GISAXS data, we report full widths at half-maximum for corresponding particle size distributions (see Figure S5 in Supporting Information).

other samples are shown in Supporting Information, Figure S3. Analysis of the GISAXS data (see Supporting Information (Note 3) for details) in the small-angle regions provides direct information about the particle size.[6,13,21,34,36] Here, to obtain the particle size distribution from GISAXS, we used IRENA software package.[72] Examples of GISAXS data fitting and obtained particle size distributions are shown in Supporting Information, Figures S4 and S5. The obtained temperature dependencies of particle sizes for clusters on ZrO_2 and ZnO are shown in Figure 5b,c, respectively, as well as in Figure S6 in Supporting Information. In Figure 5, they are compared with the NN-XANES results. For the latter, to obtain particle diameters from the obtained CN values, we interpolate the relationship between diameters and particle-averaged CNs for truncated cuboctahedral particle models (see the insets in Figures 1 and 2) with the interatomic distances in the models scaled according to the results shown in Figure 4. As mentioned before, in Figure 5, we focus only on the high-temperature range, where the particles are reduced and our NN-XANES method is applicable.

As shown in Figure 5, GISAXS results indicate unambiguously the agglomeration of the particles, previously suggested by XANES data; in all cases, the obtained particle sizes are much larger than that suggested by the nominal number of atoms, and upon temperature increase, the particle sizes increase rapidly. In Figure 5b, this trend can be seen especially

DOI: 10.1021/acs.jpcc.8b07952
J. Phys. Chem. C 2018, 122, 21686−21693

well for clusters on ZrO_2. The changes in particle sizes for particles on the ZnO support are less pronounced in this temperature range. Agglomeration for these samples takes place at lower temperatures, until the particle sizes (diameters) reach 6−8 nm, and further temperature increase does not affect the particle sizes significantly.

When GISAXS and NN-XANES results are compared, at the first glance, they point to a seeming contradiction: particle sizes, as measured by GISAXS, almost in all cases are significantly larger than those obtained from XANES analysis. Moreover, unlike it is for GISAXS data, in XANES data in the investigated temperature range and for all particles, no increase of particle size is observed. In fact, the particle sizes as obtained from XANES seem to be decreasing slightly, which we attribute to a minor artifact in our analysis because of the temperature effect in XANES data, as we explained in our previous work.[38]

The two observations can be reconciled by noting that GISAXS and XANES probe the structures at different length scales. The apparent difference between GISAXS and XANES results can be interpreted as an evidence of the granular, fractal nature of agglomerates. A similar fractal-like structure formation from soft-landed clusters has been analyzed experimentally and theoretically in the works by Bréchignac et al.[73−75] Fractal-like structures were reported also for Cu and Ag clusters inside an ultracold He matrix.[76,77] Note that GISAXS probes the form factor of the overall agglomerated particle. XANES, in turn, is sensitive to the sizes of locally ordered regions. Therefore, the larger particle sizes in GISAXS data are an indication that the agglomerates are an assembly of much smaller and locally well-ordered regions (like grapes in a grape cluster). The fact that even in the cases, where SAXS suggests a significant increase in particle sizes, the local structure and identity of the assembly-forming clusters can be well preserved may have a profound effect on our understanding of the structure−property relationship in heterogeneous catalysts in reaction conditions. For example, as demonstrated above, the Cu−Cu interatomic distance depends on the characteristic size of ordered regions (probed by XANES) rather than on the overall size of the agglomerate (probed by SAXS and, e.g., microscopy methods). One can envision that other properties (surface-induced stress, electronic structure and, consequently, catalytic properties) may be similarly more affected by the size of locally ordered regions. In the context of this work, it means that even though SAXS results show significant agglomeration of the particles, the unique properties (e.g., catalytic properties) of size-selected subnanometer clusters may be preserved in reaction conditions.

4. CONCLUSIONS

In the summary, as one important outcome of this work, we presented an approach, based on ab initio XANES simulations and artificial NN, to probe both particle size and interatomic distances in ultrasmall clusters from their in situ XANES data. This method is a promising new tool that can be used by a large number of researchers for studies of ultradispersed clusters in reaction conditions. Another result is that this new spectroscopy-based method can be combined in the same in situ experiment with a scattering probe, such as SAXS, that provides large-scale information on the clusters and their assemblies. This is particularly important because as we demonstrate in this work, the results yielded by one experimental technique only may not provide sufficient information about such complex systems as cluster assemblies on the support. The observed difference in the respective particle sizes, as yielded by SAXS and XANES methods, emphasizes the significance of combined multiprobe experiments. Simultaneously, the strong dependency of the Cu−Cu distance on the particle size, observed here for subnanometer clusters, but not for larger clusters, is a good example of the unique character of ultradispersed metallic systems and provides new routes for tailoring the properties of nanomaterials to a broad range of applications.

■ ASSOCIATED CONTENT

Supporting Information

The Supporting Information is available free of charge on the ACS Publications website at DOI: 10.1021/acs.jpcc.8b07952.

Details of ab initio XANES calculations and NN training; description of GISAXS and GIXANES experimental measurements; and supporting figures showing the validation of the NN method for distant coordination shells; additional experimental temperature-dependent XANES and SAXS data; fitting of SAXS data and temperature dependencies of particle size distributions; and average particle sizes, obtained from SAXS (PDF)

■ AUTHOR INFORMATION

Corresponding Authors

*E-mail: janis.timoshenko@gmail.com (J.T.).
*E-mail: anatoly.frenkel@stonybrook.edu (A.I.F.).

ORCID

Stefan Vajda: 0000-0002-1879-2099
Anatoly I. Frenkel: 0000-0002-5451-1207

Author Contributions

J.T. and A.H. have contributed equally to this work. J.T. and A.I.F. developed NN-based XANES analysis method and wrote the manuscript. A.H., B.Y., and S.V. designed and performed the experiments. M.J.P. performed ZnO and ZrO_2 coating of the support using atomic layer deposition. A.H. carried out analysis of SAXS data and contributed to manuscript writing. S.S. performed the experiments. All authors discussed the results and commented on the manuscript.

Notes

The authors declare no competing financial interest.

■ ACKNOWLEDGMENTS

A.I.F. acknowledges support by the U.S. Department of Energy, Office of Basic Energy Sciences under grant no. DE-FG02-03ER15476. A.I.F. acknowledges support by the Laboratory Directed Research and Development Program through LDRD 18-047 of Brookhaven National Laboratory under U.S. Department of Energy Contract No. DE-SC0012704 for initiating his research in machine learning methods. A.H., B.Y., M.J.P., and S.V. were supported by the U.S. Department of Energy, BES-Materials Science and Engineering, under Contract DE-AC-02-06CH11357, with UChicago Argonne, LLC, the operator of Argonne National Laboratory. This research used resources of the Advanced Photon Source (beamline 12-ID-C), a U.S. Department of Energy (DOE) Office of Science User Facility operated for the

DOI: 10.1021/acs.jpcc.8b07952
J. Phys. Chem. C 2018, 122, 21686−21693

DOE Office of Science by Argonne National Laboratory under Contract No. DE-AC02-06CH11357.

REFERENCES

(1) Huang, W.; Bulusu, S.; Pal, R.; Zeng, X. C.; Wang, L.-S. Structural transition of gold nanoclusters: from the golden cage to the golden pyramid. *ACS Nano* **2009**, *3*, 1225−1230.

(2) Jarrold, M. F. Nanosurface chemistry on size-selected silicon clusters. *Science* **1991**, *252*, 1085−1092.

(3) Hunter, J. M.; Fye, J. L.; Jarrold, M. F.; Bower, J. E. Structural transitions in size-selected germanium cluster ions. *Phys. Rev. Lett.* **1994**, *73*, 2063−2066.

(4) Tyo, E. C.; Vajda, S. Catalysis by clusters with precise numbers of atoms. *Nat. Nanotechnol.* **2015**, *10*, 577−588.

(5) Mammen, N.; Spanu, L.; Tyo, E. C.; Yang, B.; Halder, A.; Seifert, S.; Pellin, M. J.; Vajda, S.; Narasimhan, S. Reversing Size-Dependent Trends in the Oxidation of Copper Clusters through Support Effects. *Eur. J. Inorg. Chem.* **2018**, *2018*, 16−22.

(6) Halder, A.; Curtiss, L. A.; Fortunelli, A.; Vajda, S. Perspective: size selected clusters for catalysis and electrochemistry. *J. Chem. Phys.* **2018**, *148*, 110901.

(7) Häkkinen, H.; Yoon, B.; Landman, U.; Li, X.; Zhai, H.-J.; Wang, L.-S. On the Electronic and Atomic Structures of Small AuN-(N= 4−14) Clusters: A Photoelectron Spectroscopy and Density-Functional Study. *J. Phys. Chem. A* **2003**, *107*, 6168−6175.

(8) Jimenez-Izal, E.; Alexandrova, A. N. Computational design of clusters for catalysis. *Annu. Rev. Phys. Chem.* **2018**, *69*, 377−400.

(9) Vajda, S.; White, M. G. Catalysis applications of size-selected cluster deposition. *ACS Catal.* **2015**, *5*, 7152−7176.

(10) Kibata, T.; Mitsudome, T.; Mizugaki, T.; Jitsukawa, K.; Kaneda, K. Investigation of size-dependent properties of sub-nanometer palladium clusters encapsulated within a polyamine dendrimer. *Chem. Commun.* **2013**, *49*, 167−169.

(11) Jortner, J. Cluster size effects. *Z. Phys. D: At., Mol. Clusters* **1992**, *24*, 247−275.

(12) Schmidt, M.; Kusche, R.; von Issendorff, B.; Haberland, H. Irregular variations in the melting point of size-selected atomic clusters. *Nature* **1998**, *393*, 238−240.

(13) Lee, S.; Lee, B.; Mehmood, F.; Seifert, S.; Libera, J. A.; Elam, J. W.; Greeley, J.; Zapol, P.; Curtiss, L. A.; Pellin, M. J.; et al. Oxidative decomposition of methanol on subnanometer palladium clusters: the effect of catalyst size and support composition. *J. Phys. Chem. C* **2010**, *114*, 10342−10348.

(14) Liu, C.; Yang, B.; Tyo, E.; Seifert, S.; DeBartolo, J.; von Issendorff, B.; Zapol, P.; Vajda, S.; Curtiss, L. A. Carbon Dioxide Conversion to Methanol over Size-Selected Cu4 Clusters at Low Pressures. *J. Am. Chem. Soc.* **2015**, *137*, 8676−8679.

(15) Yang, B.; Liu, C.; Halder, A.; Tyo, E. C.; Martinson, A. B. F.; Seifert, S.; Zapol, P.; Curtiss, L. A.; Vajda, S. Copper Cluster Size Effect in Methanol Synthesis from CO2. *J. Phys. Chem. C* **2017**, *121*, 10406−10412.

(16) Yoon, B.; Häkkinen, H.; Landman, U.; Wörz, A. S.; Antonietti, J.-M.; Abbet, S.; Judai, K.; Heiz, U. Charging Effects on Bonding and Catalyzed Oxidation of CO on Au8 Clusters on MgO. *Science* **2005**, *307*, 403−407.

(17) Kaden, W. E.; Wu, T.; Kunkel, W. A.; Anderson, S. L. Electronic Structure Controls Reactivity of Size-Selected Pd Clusters Adsorbed on TiO2 Surfaces. *Science* **2009**, *326*, 826−829.

(18) Negreiros, F. R.; Halder, A.; Yin, C.; Singh, A.; Barcaro, G.; Sementa, L.; Tyo, E. C.; Pellin, M. J.; Bartling, S.; Meiwes-Broer, K.-H.; Seifert, S.; Sen, P.; Nigam, S.; Majumder, C.; Fukui, N.; Yasumatsu, H.; Vajda, S.; Fortunelli, A. Bimetallic Ag-Pt Sub-nanometer Supported Clusters as Highly Efficient and Robust Oxidation Catalysts. *Angew. Chem., Int. Ed.* **2018**, *57*, 1209−1213.

(19) Ha, M.-A.; Baxter, E. T.; Cass, A. C.; Anderson, S. L.; Alexandrova, A. N. Boron Switch for Selectivity of Catalytic Dehydrogenation on Size-Selected Pt Clusters on Al2O3. *J. Am. Chem. Soc.* **2017**, *139*, 11568−11575.

(20) Gota, S.; Gautier, M.; Douillard, L.; Thromat, N.; Duraud, J. P.; Le Fèvre, P. Influence of the substrate oxidation state in the growth of copper clusters on Al2O3(0001) surface: a XANES and EXAFS study. *Surf. Sci.* **1995**, *323*, 163−174.

(21) Wyrzgol, S. A.; Schäfer, S.; Lee, S.; Lee, B.; Vece, M. D.; Li, X.; Seifert, S.; Winans, R. E.; Stutzmann, M.; Lercher, J. A.; et al. Combined TPRx, in situ GISAXS and GIXAS studies of model semiconductor-supported platinum catalysts in the hydrogenation of ethene. *Phys. Chem. Chem. Phys.* **2010**, *12*, 5585−5595.

(22) Kim, D.; Becknell, N.; Yu, Y.; Yang, P. Room-temperature dynamics of vanishing copper nanoparticles supported on silica. *Nano Lett.* **2017**, *17*, 2732−2737.

(23) Porsgaard, S.; Merte, L. R.; Ono, L. K.; Behafarid, F.; Matos, J.; Helveg, S.; Salmeron, M.; Cuenya, B. R.; Besenbacher, F. Stability of Platinum Nanoparticles Supported on SiO2/Si(111): A High-Pressure X-ray Photoelectron Spectroscopy Study. *ACS Nano* **2012**, *6*, 10743−10749.

(24) Viswanath, B.; Patra, S.; Munichandraiah, N.; Ravishankar, N. Nanoporous Pt with High Surface Area by Reaction-Limited Aggregation of Nanoparticles. *Langmuir* **2009**, *25*, 3115−3121.

(25) Roese, S.; Kononov, A.; Timoshenko, J.; Frenkel, A. I.; Hövel, H. Cluster assemblies produced by aggregation of preformed Ag clusters in ionic liquids. *Langmuir* **2018**, *34*, 4811−4819.

(26) Lei, Y.; Mehmood, F.; Lee, S.; Greeley, J.; Lee, B.; Seifert, S.; Winans, R. E.; Elam, J. W.; Meyer, R. J.; Redfern, P. C.; Teschner, D.; Schlogl, R.; Pellin, M. J.; Curtiss, L. A.; Vajda, S. Increased silver activity for direct propylene epoxidation via subnanometer size effects. *Science* **2010**, *328*, 224−228.

(27) Cheng, L.; Yin, C.; Mehmood, F.; Liu, B.; Greeley, J.; Lee, S.; Lee, B.; Seifert, S.; Winans, R. E.; Teschner, D.; Schlögl, R.; Vajda, S.; Curtiss, L. A. Reaction mechanism for direct propylene epoxidation by alumina-supported silver aggregates: the role of the particle/support interface. *ACS Catal.* **2013**, *4*, 32−39.

(28) Rehr, J. J.; Albers, R. C. Theoretical approaches to X-ray absorption fine structure. *Rev. Mod. Phys.* **2000**, *72*, 621−654.

(29) Sayers, D. E.; Stern, E. A.; Lytle, F. W. New Technique for Investigating Noncrystalline Structures: Fourier Analysis of the Extended X-Ray-Absorption Fine Structure. *Phys. Rev. Lett.* **1971**, *27*, 1204−1207.

(30) Frenkel, A. I. Solving the structure of nanoparticles by multiple-scattering EXAFS analysis. *J. Synchrotron Radiat.* **1999**, *6*, 293−295.

(31) Frenkel, A. Solving the 3D structure of metal nanoparticles. *Z. Kristallogr.* **2007**, *222*, 605−611.

(32) Frenkel, A. I.; Yevick, A.; Cooper, C.; Vasic, R. Modeling the structure and composition of nanoparticles by extended X-ray absorption fine-structure spectroscopy. *Annu. Rev. Anal. Chem.* **2011**, *4*, 23−39.

(33) Frenkel, A. I. Applications of extended X-ray absorption fine-structure spectroscopy to studies of bimetallic nanoparticle catalysts. *Chem. Soc. Rev.* **2012**, *41*, 8163−8178.

(34) Renaud, G.; Lazzari, R.; Revenant, C.; Barbier, A.; Noblet, M.; Ulrich, O.; Leroy, F.; Jupille, J.; Borensztein, Y.; Henry, C. R. Real-time monitoring of growing nanoparticles. *Science* **2003**, *300*, 1416−1419.

(35) Lee, S.; Lee, B.; Seifert, S.; Vajda, S.; Winans, R. E. Simultaneous measurement of X-ray small angle scattering, absorption and reactivity: A continuous flow catalysis reactor. *Nucl. Instrum. Methods Phys. Res., Sect. A* **2011**, *649*, 200−203.

(36) Winans, R. E.; Vajda, S.; Ballentine, G. E.; Elam, J. W.; Lee, B.; Pellin, M. J.; Seifert, S.; Tikhonov, G. Y.; Tomczyk, N. A. Reactivity of supported platinum nanoclusters studied by in situ GISAXS: clusters stability under hydrogen. *Top. Catal.* **2006**, *39*, 145−149.

(37) Dai, Y.; Gorey, T. J.; Anderson, S. L.; Lee, S.; Lee, S.; Seifert, S.; Winans, R. E. Inherent size effects on XANES of nanometer metal clusters: size-selected platinum clusters on silica. *J. Phys. Chem. C* **2016**, *121*, 361−374.

(38) Timoshenko, J.; Lu, D.; Lin, Y.; Frenkel, A. I. Supervised Machine-Learning-Based Determination of Three-Dimensional Struc-

DOI: 10.1021/acs.jpcc.8b07952
J. Phys. Chem. C 2018, 122, 21686−21693

ture of Metallic Nanoparticles. *J. Phys. Chem. Lett.* **2017**, *8*, 5091−5098.
(39) Hori, Y. i. Electrochemical CO_2 reduction on metal electrodes. *Modern Aspects of Electrochemistry*; Springer, 2008; pp 89−189.
(40) Hoang, T. T. H.; Verma, S.; Ma, S.; Fister, T. T.; Timoshenko, J.; Frenkel, A. I.; Kenis, P. J. A.; Gewirth, A. A. Nanoporous Copper-Silver Alloys by Additive-Controlled Electrodeposition for the Selective Electroreduction of CO2 to Ethylene and Ethanol. *J. Am. Chem. Soc.* **2018**, *140*, 5791−5797.
(41) Grosse, P.; Gao, D.; Scholten, F.; Sinev, I.; Mistry, H.; Cuenya, B. R. Dynamic Changes in the Structure, Chemical State and Catalytic Selectivity of Cu Nanocubes during CO2 Electroreduction: Size and Support Effects. *Angew. Chem.* **2018**, *130*, 6300−6305.
(42) Zhou, Y.; Jin, C.; Li, Y.; Shen, W. Dynamic behavior of metal nanoparticles for catalysis. *Nano Today* **2018**, *20*, 101−120.
(43) Xie, H.; Wang, T.; Liang, J.; Li, Q.; Sun, S. Cu-based nanocatalysts for electrochemical reduction of CO 2. *Nano Today* **2018**, *21*, 41−54.
(44) Apai, G.; Hamilton, J. F.; Stohr, J.; Thompson, A. Extended X-Ray-Absorption Fine Structure of Small Cu and Ni Clusters: Binding-Energy and Bond-Length Changes with Cluster Size. *Phys. Rev. Lett.* **1979**, *43*, 165−169.
(45) Tománek, D.; Mukherjee, S.; Bennemann, K. H. Simple theory for the electronic and atomic structure of small clusters. *Phys. Rev. B: Condens. Matter Mater. Phys.* **1983**, *28*, 665−673.
(46) Frenkel, A. I.; Nemzer, S.; Pister, I.; Soussan, L.; Harris, T.; Sun, Y.; Rafailovich, M. H. Size-controlled synthesis and characterization of thiol-stabilized gold nanoparticles. *J. Chem. Phys.* **2005**, *123*, 184701.
(47) Mays, C. W.; Vermaak, J. S.; Kuhlmann-Wilsdorf, D. On surface stress and surface tension. *Surf. Sci.* **1968**, *12*, 134−140.
(48) Richter, B.; Kuhlenbeck, H.; Freund, H.-J.; Bagus, P. S. Cluster core-level binding-energy shifts: the role of lattice strain. *Phys. Rev. Lett.* **2004**, *93*, 026805.
(49) Aruna, I.; Mehta, B. R.; Malhotra, L. K.; Shivaprasad, S. M. Size dependence of core and valence binding energies in Pd nanoparticles: interplay of quantum confinement and coordination reduction. *J. Appl. Phys.* **2008**, *104*, 064308.
(50) Strasser, P.; Koh, S.; Anniyev, T.; Greeley, J.; More, K.; Yu, C.; Liu, Z.; Kaya, S.; Nordlund, D.; Ogasawara, H.; Toney, M. F.; Nilsson, A. Lattice-strain control of the activity in dealloyed core-shell fuel cell catalysts. *Nat. Chem.* **2010**, *2*, 454−460.
(51) Jalan, V.; Taylor, E. Importance of interatomic spacing in catalytic reduction of oxygen in phosphoric acid. *J. Electrochem. Soc.* **1983**, *130*, 2299−2302.
(52) Hansen, L. B.; Stoltze, P.; Nørskov, J. K.; Clausen, B. S.; Niemann, W. Is there a contraction of the interatomic distance in small metal particles? *Phys. Rev. Lett.* **1990**, *64*, 3155−3158.
(53) Clausen, B. S.; Topsøe, H.; Hansen, L. B.; Stoltze, P.; Nørskov, J. K. The effect of anharmonicity on the EXAFS coordination number in small metallic particles. *Jpn. J. Appl. Phys.* **1993**, *32*, 95.
(54) Clausen, B. S.; Grabaek, L.; Topsoe, H.; Hansen, L. B.; Stoltze, P.; Norskov, J. K.; Nielsen, O. H. A new procedure for particle size determination by EXAFS based on molecular dynamics simulations. *J. Catal.* **1993**, *141*, 368−379.
(55) Clausen, B. S.; Topsøe, H.; Hansen, L. B.; Stoltze, P.; Nørskov, J. K. Determination of metal particle sizes from EXAFS. *Catal. Today* **1994**, *21*, 49−55.
(56) Clausen, B. S.; Nørskov, J. K. Asymmetric pair distribution functions in catalysts. *Top. Catal.* **2000**, *10*, 221−230.
(57) Timoshenko, J.; Frenkel, A. I. Probing structural relaxation in nanosized catalysts by combining EXAFS and reverse Monte Carlo methods. *Catal. Today* **2017**, *280*, 274−282.
(58) Bazin, D.; Rehr, J. J. Limits and advantages of X-ray absorption near edge structure for nanometer scale metallic clusters. *J. Phys. Chem. B* **2003**, *107*, 12398−12402.
(59) Oyanagi, H.; Sun, Z. H.; Jiang, Y.; Uehara, M.; Nakamura, H.; Yamashita, K.; Orimoto, Y.; Zhang, L.; Lee, C.; Fukano, A.; Maeda, H. Small copper clusters studied by x-ray absorption near-edge structure. *J. Appl. Phys.* **2012**, *111*, 084315.
(60) Rehr, J. J.; Kas, J. J.; Vila, F. D.; Prange, M. P.; Jorissen, K. Parameter-free calculations of X-ray spectra with FEFF9. *Phys. Chem. Chem. Phys.* **2010**, *12*, 5503−5513.
(61) Myers, V. S.; Weir, M. G.; Carino, E. V.; Yancey, D. F.; Pande, S.; Crooks, R. M. Dendrimer-encapsulated nanoparticles: new synthetic and characterization methods and catalytic applications. *Chem. Sci.* **2011**, *2*, 1632−1646.
(62) Bunău, O.; Joly, Y. Self-consistent aspects of X-ray absorption calculations. *J. Phys.: Condens. Matter* **2009**, *21*, 345501.
(63) Straumanis, M. E.; Yu, L. S. Lattice parameters, densities, expansion coefficients and perfection of structure of Cu and of Cu-In α phase. *Acta Crystallogr., Sect. A: Cryst. Phys., Diffr., Theor. Gen. Crystallogr.* **1969**, *25*, 676−682.
(64) Glasner, D.; Frenkel, A. I. Geometrical characteristics of regular polyhedra: application to EXAFS studies of nanoclusters. *AIP Conf. Proc.* **2007**, *882*, 746−748.
(65) Montano, P. A.; Shenoy, G. K.; Alp, E. E.; Schulze, W.; Urban, J. Structure of copper microclusters isolated in solid argon. *Phys. Rev. Lett.* **1986**, *56*, 2076−2079.
(66) Timoshenko, J.; Anspoks, A.; Cintins, A.; Kuzmin, A.; Purans, J.; Frenkel, A. I. Neural network approach for characterizing structural transformations by X-ray absorption fine structure spectroscopy. *Phys. Rev. Lett.* **2018**, *120*, 225502.
(67) Ravel, B.; Newville, M. ATHENA, ARTEMIS, HEPHAESTUS: data analysis for X-ray absorption spectroscopy using IFEFFIT. *J. Synchrotron Radiat.* **2005**, *12*, 537−541.
(68) O'Neill, B. J.; Jackson, D. H.; Lee, J.; Canlas, C.; Stair, P. C.; Marshall, C. L.; Elam, J. W.; Kuech, T. F.; Dumesic, J. A.; Huber, G. W. Catalyst design with atomic layer deposition. *ACS Catal.* **2015**, *5*, 1804−1825.
(69) Tynell, T.; Karppinen, M. Atomic layer deposition of ZnO: a review. *Semicond. Sci. Technol.* **2014**, *29*, 043001.
(70) Jayanetti, S.; Mayanovic, R. A.; Anderson, A. J.; Bassett, W. A.; Chou, I.-M. Analysis of radiation-induced small Cu particle cluster formation in aqueous CuCl2. *J. Chem. Phys.* **2001**, *115*, 954−962.
(71) Oyanagi, H.; Orimoto, Y.; Hayakawa, K.; Hatada, K.; Sun, Z. H.; Zhang, L.; Yamashita, K.; Nakamura, H.; Uehara, M.; Fukano, A.; et al. Nanoclusters synthesized by synchrotron radiolysis in concert with wet chemistry. *Sci. Rep.* **2014**, *4*, 7199.
(72) Ilavsky, J.; Jemian, P. R. Irena: tool suite for modeling and analysis of small-angle scattering. *J. Appl. Crystallogr.* **2009**, *42*, 347−353.
(73) Bréchignac, C.; Cahuzac, P.; Carlier, F.; Colliex, C.; de Frutos, M.; Kébaïli, N.; Le Roux, J.; Masson, A.; Yoon, B. Control of island morphology by dynamic coalescence of soft-landed clusters. *Eur. Phys. J. D* **2001**, *16*, 265−269.
(74) Bréchignac, C.; Cahuzac, P.; Carlier, F.; Colliex, C.; de Frutos, M.; Kébaïli, N.; Le Roux, J.; Masson, A.; Yoon, B. Thermal and chemical nanofractal relaxation. *Eur. Phys. J. D* **2003**, *24*, 265−268.
(75) Solov'yov, I. A.; Solov'yov, A. V.; Kébaili, N.; Masson, A.; Bréchignac, C. Thermally induced morphological transition of silver fractals. *Phys. Status Solidi B* **2014**, *251*, 609−622.
(76) Loginov, E.; Gomez, L. F.; Chiang, N.; Halder, A.; Guggemos, N.; Kresin, V. V.; Vilesov, A. F. Photoabsorption of Ag_N (N∼ 6−6000) nanoclusters formed in helium droplets: transition from compact to multicenter aggregation. *Phys. Rev. Lett.* **2011**, *106*, 233401.
(77) Gomez, L. F.; Loginov, E.; Halder, A.; Kresin, V. V.; Vilesov, A. F. Formation of unusual copper clusters in helium nanodroplets. *Int. J. Nanosci.* **2013**, *12*, 1350014.

DOI: 10.1021/acs.jpcc.8b07952
J. Phys. Chem. C 2018, 122, 21686−21693